Journal of Solid State Chemistry 184 (2011) 2812–2817

Contents lists available at SciVerse ScienceDirect

Journal of Solid State Chemistry

journal homepage: www.elsevier.com/locate/jssc

# Pressure-induced phase transitions in multiferroic $RbFe(MoO_4)_2$—Raman scattering study

M. Mączka [a,*], M. Ptak [a], C. Luz-Lima [b], P.T.C. Freire [b], W. Paraguassu [c], S. Guerini [d], J. Hanuza [e]

[a] Institute of Low Temperature and Structure Research, Polish Academy of Sciences, P.O. Box 1410, 50-950 Wrocław 2, Poland
[b] Departamento de Física, Universidade Federal do Ceara, Fortaleza, Ceara, Brazil
[c] Faculdade de Física, Universidade Federal do Pará, 66075-110 Belém, PA, Brazil
[d] Departamento de Fisica, Universidade Federal do Maranhão, São Luis-MA 65085-580, Brazil
[e] Department of Bioorganic Chemistry, University of Economics, 53-345 Wroclaw, Poland

ARTICLE INFO

*Article history:*
Received 25 July 2011
Received in revised form
22 August 2011
Accepted 23 August 2011
Available online 1 September 2011

*Keywords:*
Lattice dynamics
High pressure
Phase transitions

ABSTRACT

High pressure Raman scattering experiments were performed on $RbFe(MoO_4)_2$. These experiments revealed that two phase transitions take place in $RbFe(MoO_4)_2$ at very low pressures, i.e. between ambient pressure and 0.2 GPa and between 0.4 and 0.7 GPa. Raman results showed that at the first phase transition the room temperature $P\bar{3}m1$ phase transforms into the $P\bar{3}$ phase, which is also observed at ambient pressure below 190 K. The second pressure-induced phase transition occurs into a low symmetry phase of unknown symmetry. The performed lattice dynamics calculations for the $P\bar{3}m1$ phase and *ab initio* calculation of the structural changes under hydrostatic pressure helped us to get better insights into the mechanism of the observed phase transitions.



## 1. Introduction

$RbFe(MoO_4)_2$ belongs to the family of layered trigonal molybdates and tungstates with chemical formula $M^+M^{3+}(MoO_4)_2$, where $M^+$=Na, K, Rb, Cs and $M^{3+}$=Al, Sc, Cr, Fe [1–3]. These materials are potential candidates for broadband laser applications [4]. Iron containing molybdates, $KFe(MoO_4)_2$ and $RbFe(MoO_4)_2$, also gained considerable attention due to the fact that they constitute rare examples of nearly two-dimensional "triangular" antiferromagnets available in single crystal form [5–9]. Recently, it has been found that $RbFe(MoO_4)_2$ belongs to the group of multiferroic materials with a simultaneous onset of magnetic and ferroelectric order [10].

The crystal structure of $RbFe(MoO_4)_2$ was shown to be isotypic with $KAl(MoO_4)_2$ having symmetry of the space group $P\bar{3}m1$ [11,12]. In this structure type the magnetic ions substituting $Al^{3+}$ are located in triangular nets, which are stacked in separated layers arranged perpendicular to the *c*-axis, and the Rb atoms occupy the interlayer space. $RbFe(MoO_4)_2$ exhibits a structural phase transition at $T_c$=190 K, which was revealed by electron spin resonance (ESR), Raman spectroscopy and X-ray powder diffraction (XPD) [5]. Based on the neutron powder diffraction analysis, it was assumed that below 190 K temperature the symmetry changes to $P\bar{3}$ [8]. Recently, we have confirmed this symmetry by temperature dependent single crystal X-ray diffraction studies [12].

High-pressure studies are very important for understanding structural instabilities of materials. As far as iron containing compounds are concerned, we have reported high-pressure studies on $KFe(MoO_4)_2$, which revealed three pressure induced phase transitions from the monoclinic ambient pressure phase at about 0.25 GPa, 1.3 GPa and 1.6 GPa [13]. The phase stable between 0.25 and 1.3 GPa was shown to have $P\bar{3}m1$ symmetry [13]. The phase stable in the 1.3–1.6 GPa is trigonal and we proposed that it might be described by the $P\bar{3}c1$ space group. Symmetry of the phase stable above 1.6 GPa is not known but it is most likely triclinic [13]. Regarding $RbFe(MoO_4)_2$, we have performed high-pressure X-ray powder diffraction study for this material [12]. This study showed that amorphization starts above 5 GPa and increases gradually on further pressure increase suggesting the thermodynamic instability of the high-pressure phase [12].

In the present paper, we report high-pressure Raman scattering studies of $RbFe(MoO_4)_2$ in order to obtain information on the structural changes occurring in this crystal under hydrostatic pressure and the pressure dependence of the phonon properties. We have also carried out lattice dynamics calculations for the ambient pressure phase and *ab initio* calculations of the structural changes under hydrostatic pressure.

## 2. Experimental

Single crystals of $RbFe(MoO_4)_2$ were grown by the flux method. The mixture of $Rb_2CO_3$, $Fe_2O_3$ and $MoO_3$ (Fluka products) corresponding to the ratio 2:1:6 was placed in a platinum crucible,

* Corresponding author. Fax: +48 71 3441029.
*E-mail address:* m.maczka@int.pan.wroc.pl (M. Mączka).

0022-4596/$ - see front matter © 2011 Elsevier Inc. All rights reserved.
doi:10.1016/j.jssc.2011.08.032

heated to 800 °C and kept at this temperature for 40 h. Next, the melt was cooled at a rate of 2 °C/h to 500 °C and then cooled at a rate of 5 °C/h to room temperature. The obtained crystals of optical quality were extracted from the crucible by washing with hot water.

The light-yellow-green transparent crystals of a plate-like shape with typical dimensions $0.3 \times 0.2 \times 0.15$ cm$^3$ were obtained. The chemical composition of the obtained crystals was checked using microprobe analyzer (Philips SEM 515) and EDAX spectrometer (PV 9800).

The Raman spectra were obtained with a triple-grating spectrometer Jobin Yvon T64000, which is equipped with a $N_2$-cooled charge coupled device detection system. The 514.5 nm line of an argon laser was used for excitation. The laser power was 80 mW and the power on the sample in the cell was about 2 mW. The scattering geometry was $z(xx+xy)z$. An Olympus microscope lens with a focal distance of 20.5 mm and a numerical aperture of 0.35 was used to focus the laser beam on the sample surface. The high-pressure experiments were performed using a diamond anvil cell with a 4:1 methanol:ethanol mixture as the transmission fluid. Pressures were measured based on the shifts of the ruby R1 and R2 fluorescence lines. The spectrometer slits were set for a resolution of 2 cm$^{-1}$.

## 3. Results and discussion

### 3.1. Lattice dynamics calculations and assignment of modes

A standard group theoretical analysis for the $P\bar{3}m1$ ambient pressure phase of $RbFe(MoO_4)_2$ containing 12 atoms in the unit cell ($Rb^+$ ions at 1*b* sites, $Fe^{3+}$ ions at 1*a* sites, Mo atoms at 2*d* sites, O1 atoms at 2*d* sites and O2 atoms at 6*i* sites [12]) leads to 36 degrees of freedom at the Brillouin zone center ($\Gamma$ point). The optical modes are distributed among the irreducible representations of the factor group $D_{3d}$ as $4A_{1g}+5E_g+A_{2g}+5A_{2u}+6E_u+A_{1u}$. Selection rules state that $A_{1g}$ and $E_g$ modes are Raman active, the $A_{2u}$ and $E_u$ modes are IR active, $A_{2g}$ and $A_{1u}$ modes are silent. These modes can be subdivided into $\nu_1$ symmetric stretching ($A_{1g}+A_{2u}$), $\nu_3$ antisymmetric stretching ($A_{1g}+E_g+A_{2u}+E_u$), $\nu_2$ symmetric bending ($E_g+E_u$), $\nu_4$ antisymmetric bending ($A_{1g}+E_g+A_{2u}+E_u$), translational ($A_{1g}+E_g$) and librational ($E_g+A_{2g}+E_u+A_{1u}$) modes of the $MoO_4^{2-}$ ions as well as translational modes of $Rb^+$ cations ($A_{2u}+E_u$) and coupled translational modes of the $MoO_4^{2-}$ and $Fe^{3+}$ ions ($A_{2u}+E_u$).

In order to get insight into the vibrational properties of $RbFe(MoO_4)_2$, we have performed lattice dynamics calculations for the room temperature $P\bar{3}m1$ structure. These calculations were performed using GULP code developed by Gale [14]. We have determined a set of classical ionic pair potential that better optimizes the $RbFe(MoO_4)_2$ structure. The obtained set of potential parameters has been then used to derive the initial force constants that were refined using Wilson's FG matrix method and the software package VIBRATZ developed by Dowty [15].

The ionic shell model used in the GULP code treats the material as a collection of core–shell systems (symbolizing nuclei and electron shell) interacting with each other through electrostatic and short-range classic potentials. This model was successfully used for a number of molybdate and tungstate based systems [13,16,17]. The following inter-atomic potential is taken into account:

$$U_{ij}(r_{ij}) = \frac{z_i z_j e^2}{r_{ij}} + b_{ij}\exp\left[\frac{-r_{ij}}{\rho_{ij}}\right] - \frac{c_{ij}}{r_{ij}^6} \quad (1)$$

The first term is related to the Coulomb forces for modeling the long-range interactions. The second term is related to the Born–Mayer type repulsive interaction for accounting the short-range forces. A van der Waals attractive interaction (third term) is modeled by the dipole–dipole interaction. $z_i$ and $z_j$ are the effective charges of the *i* and the *j* ions, respectively, separated by the distance $r_{ij}$. The parameters $\rho_{ij}$ and $b_{ij}$ correspond to the ionic radii and ionic stiffness, respectively. The initial lattice parameters and atomic positions for the $RbFe(MoO_4)_2$ structure were taken from the experimental data [12]. The optimized potential parameters and ionic charges obtained after energy minimization are listed in Table 1. Using this set of parameters, a good agreement between the calculated and the experimental lattice parameters for the $P\bar{3}m1$ space group was obtained with volumetric error within 1.5%.

As previously pointed, the phonon calculations were performed using Wilson's FG matrix method and the software package VIBRATZ developed by Dowty [15]. The initial force constants were obtained using the relation:

$$f_{ij} = -\frac{1}{r}\frac{\partial U_{ij}(r)}{\partial r} \quad (2)$$

where the indices *i* and *j* refer to interacting ions, and *r* is the distance between them. In order to better fit the experimental data, the obtained force constant values were refined. This procedure is necessary in order to correct the lack of covalence in the ionic model. The final values of force constants used in the calculation are listed in Table 2.

Table 3 lists the experimental and the calculated wavenumbers together with the proposed assignment. Experimental IR wavenumbers were taken from Ref. [12]. Fig. 1 illustrates atomic displacements for several Raman-active normal modes of $RbFe(MoO_4)_2$ at ambient phase. The performed calculations confirm that the Raman and IR bands in the 765–977 and 302–388 cm$^{-1}$ range correspond to stretching and bending vibrations of the $MoO_4$ tetrahedral units, respectively. They also show that the IR modes at 235 and 256 cm$^{-1}$ correspond to coupled translations of the $Fe^{3+}$ and $MoO_4^{2-}$ ions. Translational modes of $Rb^+$ ions give rise to IR bands at 98 and 150 cm$^{-1}$. IR active librational mode is observed at 188 cm$^{-1}$ and our calculations show that the Raman active librational mode is strongly coupled to translational mode of the $MoO_4^{2-}$ ions giving rise to two Raman bands at 51 and 168 cm$^{-1}$. Pure translational mode of the $MoO_4^{2-}$ ions is observed in the Raman spectra at 150 cm$^{-1}$.

**Table 1**
Potential parameters (see Eq. (1) in the text) and ionic charges used in the lattice dynamics calculation.

| Interaction | *b* (eV) | *ρ* (Å) | *c* (eV Å$^6$) |
|---|---|---|---|
| **Buckingham** | | | |
| Mo–O | 2023.97 | 0.347 | 0 |
| Fe–O | 3163.945 | 0.2641 | 0 |
| Rb–O | 2665.507 | 0.326 | 0 |
| O-O | 9547.96 | 0.2192 | 32 |
| **Charges** | | | |
| $Z_{Rb}=1$; $Z_{Fe}=3$; $Z_{Mo}=6$; $Z_O=-2.0$ | | | |

**Table 2**
Force constants used in the phonon calculations.

| Bond | Distance (Å)/force (mdyn/Å) |
|---|---|
| Mo–O | 1.7065/7.0 |
| | 1.7651/3.2 |
| Fe–O | 1.9777/1.5 |
| Rb–O | 3.0–3.28/0.12–0.11 |
| O–O | 2.75 – 3.33/0.44–0.24 |

### 3.2. High pressure Raman scattering study

Once a clear picture of the vibrational properties of RbFe$(MoO_4)_2$ is obtained we next discuss the effects of hydrostatic pressure on the structural and vibrational properties of this compound. Pressure dependence of Raman spectra is shown in Figs. 2 and 3. However, the overall changes in the Raman spectra can be better followed by analyzing the wavenumber ($\omega$) vs. pressure ($P$) plot shown in Fig. 4. Fig. 4 shows that the pressure dependence of all Raman-active modes, except of that at 51 $cm^{-1}$, can be well described using a linear function $\omega(P)=\omega_0+\alpha P$. The values of $\omega_0$ and $\alpha$ are collected in Table 4.

Figs. 2 and 3 show that sudden change in the Raman spectrum occurs already at 0.2 GPa. The most characteristic change is strong intensity increase of the 360 $cm^{-1}$ band. This change indicates

**Table 3**
Experimental and calculated wavenumbers for $RbFe(MoO_4)_2$ together with the proposed assignment.

| Sym. | Exp. | Calc. | Sym. | Exp. | Calc. [12] | Assignment |
|---|---|---|---|---|---|---|
| $A_{1g}$ | 977 | 976 | $A_{2u}$ | 952 | 973 | $\nu_1$ |
| $A_{1g}$ | 930 | 897 | $A_{2u}$ | 921 | 880 | $\nu_3$ |
| $E_g$ | 765 | 800 | $E_u$ | 824 | 836 | $\nu_3$ |
| $E_g$ | 360 | 371 | $E_u$ | 388 | 353 | $\nu_4$ |
| $A_{1g}$ | 343 | 383 | $A_{2u}$ | 326 | 336 | $\nu_4$ |
| $E_g$ | 338 | 335 | $E_u$ | 302 | 377 | $\nu_2$ |
| | | | $E_u$ | 256 | 258 | T′(Fe)*T′($MoO_4$) |
| | | | $A_{1u}$ | - | 216 | L($MoO_4$) |
| | | | $A_{2u}$ | 235 | 213 | T′(Fe)*T′($MoO_4$) |
| | | | $E_u$ | 188 | 195 | L($MoO_4$) |
| $E_g$ | 168 | 217 | | | | T′($MoO_4$)* L($MoO_4$) |
| $A_{1g}$ | 150 | 127 | | | | T′($MoO_4$) |
| | | | $A_{2u}$ | 150 | 105 | T′(Rb) |
| | | | $E_u$ | 98 | 84 | T′(Rb) |
| $E_g$ | 51 | 85 | | | | T′($MoO_4$)* L($MoO_4$) |
| $A_{2g}$ | – | 80 | | | | L($MoO_4$) |

*Note*: * means "coupled to".

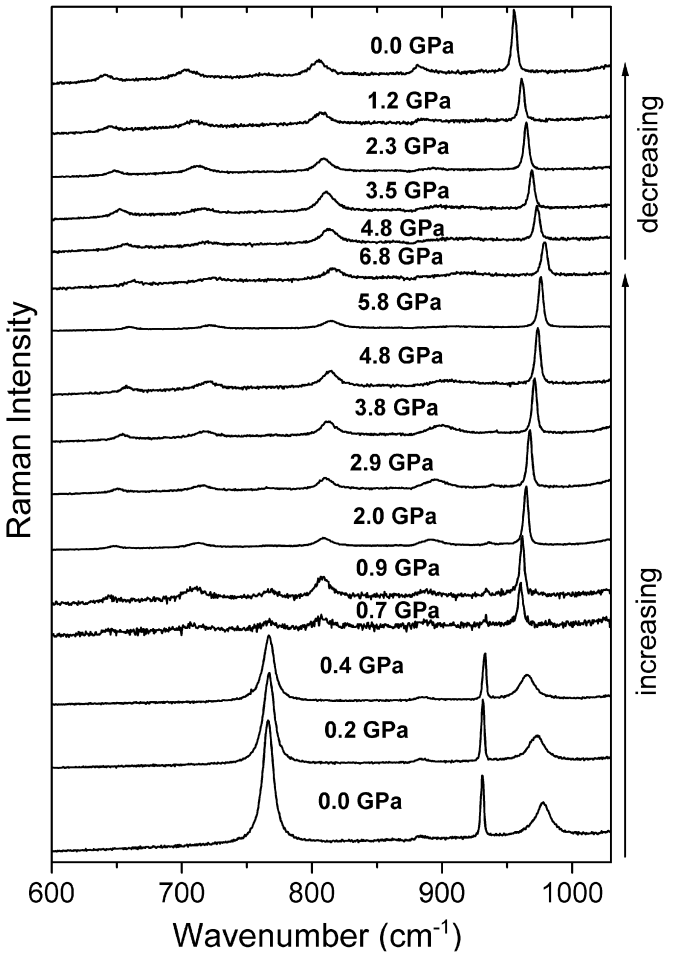


**Fig. 2.** Raman spectra of $RbFe(MoO_4)_2$ crystal in the high wavenumber region recorded at different pressures during compression and decompression experiments.

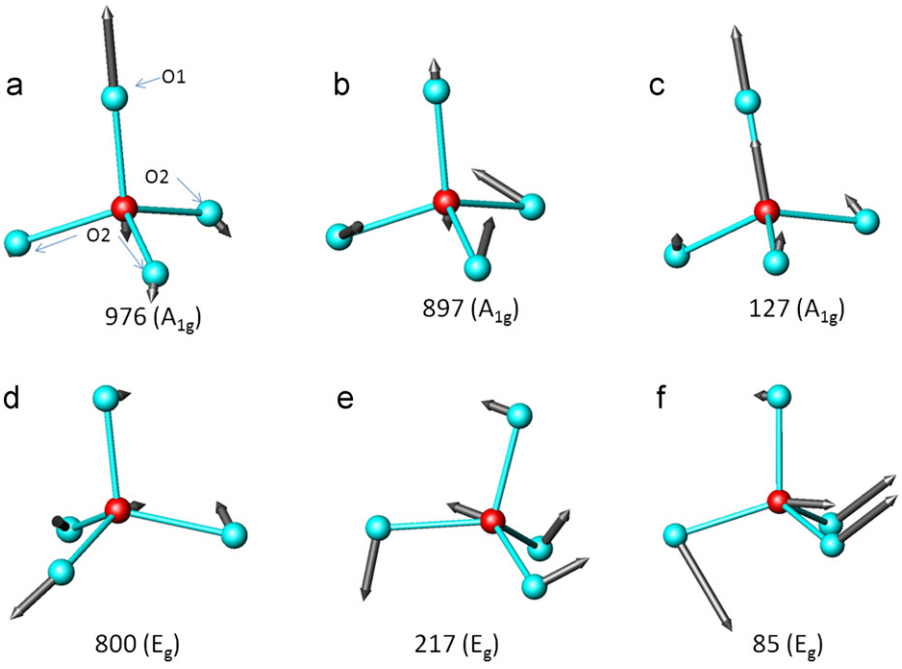


**Fig. 1.** Atomic displacements for several Raman-active normal modes of $RbFe(MoO_4)_2$ at ambient phase.

that a first pressure-induced phase transition took place somewhere between ambient pressure and 0.2 GPa. Unfortunately, the available diamond anvil cells do not allow to obtain additional experimental points between 0 and 0.2 GPa and, therefore, more precise information of transition pressure could not be obtained.

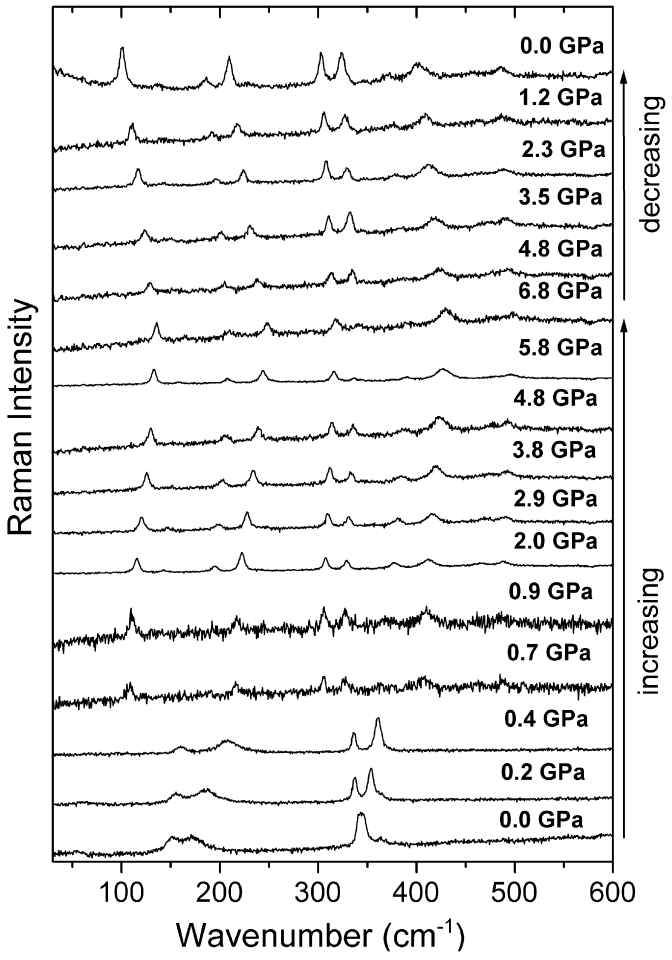


**Fig. 3.** Raman spectra of $RbFe(MoO_4)_2$ crystal in the low wavenumber region recorded at different pressures during compression and decompression experiments.

By further increasing the pressure, wavenumbers of majority of modes increase (see Figs. 2–4). The pressure coefficients $\alpha$ are unusually large for some modes, especially for the $\omega_0=163\ cm^{-1}$ mode, in agreement with the extreme softness of this material, as previously reported [12]. However, negative pressure dependence is observed for the modes with $\omega_0$ equal to 980 and 338 $cm^{-1}$.

Raman spectra experience drastic changes also at 0.7 GPa indicating that a second phase transition took place between 0.4 and 0.7 GPa. The most characteristic features of this phase transition are (i) large and discontinuous frequency shifts; (ii) large intensity change of all modes; (iii) increase in the number of observed bands from 8 to 14 and (iv) decrease of the energy gap between stretching and bending modes from about 350 to 150 $cm^{-1}$. Upon further increase of pressure, the spectra remain qualitatively the same, indicating that this high-pressure phase is stable up to 6.8 GPa, the highest pressure reached in our experiment.

In order to get a new insight into the mechanism of phase transitions in $RbFe(MoO_4)_2$, we have also performed Raman studies of $RbFe(MoO_4)_2$ crystal during the decompression. This study shows that upon releasing the pressure, the starting $P\bar{3}m1$ phase was not recovered (see Figs. 2 and 3). This result indicates that the transition into the high-pressure phase is not reversible.

### 3.3. *Ab initio calculations*

In order to shed light on observed modifications in the Raman spectra, first principle density-functional theory (DFT) calculations were performed to study the structural changes undergone by the $P\bar{3}m1$ phase of $RbFe(MoO_4)_2$ system under hydrostatic pressure [18]. The SIESTA code was used, and full self-consistent calculations were performed by solving the Kohn Sham equations [19,20]. The local density approximation of Perdew–Zunger was employed to the exchange and correlation functional and double zeta basis plus polarization was used to represent the valence electrons [21,22]. The interaction between ionic cores and valence electrons is described by norm conserving pseudopotentials [23], in the Kleinman–Bylander form [24]. A cut-off of 150 Ry for the

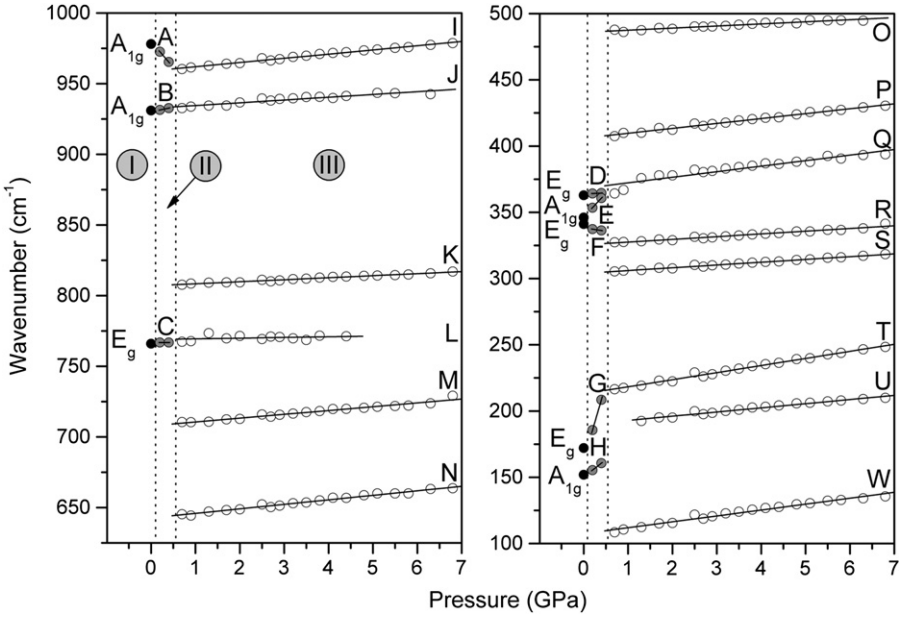


**Fig. 4.** Frequency vs. pressure plot in the high frequency (left panel) and low frequency (right panel) region observed during compression. The solid lines are linear fits of the data to $\omega(P)=\omega_0+\alpha P$. The vertical lines indicate the pressures at which the phase transitions take place.

**Table 4**
Pressure intercepts $\omega_0$ and pressure coefficients $\alpha$ for high pressure phases of $RbFe(MoO_4)_2$. For the $P\bar{3}m1$ phase, the ambient pressure and room temperature values are given.

| NTP phase Phase I | | Low pressure phase Phase II | | | High pressure phase Phase II | | | Assignment |
|---|---|---|---|---|---|---|---|---|
| Band | Wavenumber ($cm^{-1}$) | Band | $\omega_0$ ($cm^{-1}$) | $\alpha$ ($cm^{-1}$ $GPa^{-1}$) | Band | $\omega_0$ ($cm^{-1}$) | $\alpha$ ($cm^{-1}$ $GPa^{-1}$) | |
| $\omega(P)=\omega_0+\alpha P$ | | | | | | | | |
| $A_{1g}$ | 977 | *A* | 979.9 | −36.5 | *I* | 959.0 | 3.0 | $\nu_1(MoO_4)$ |
| $A_{1g}$ | 930 | *B* | 930.1 | 6.5 | *J* | 932.5 | 2.0 | $\nu_3(MoO_4)$ |
| | | | | | *K* | 807.0 | 1.4 | |
| $E_g$ | 765 | *C* | 766.8 | 0.0 | *L* | 768.9 | 0.5 | |
| | | | | | *M* | 707.8 | 2.7 | |
| | | | | | *N* | 642.7 | 3.2 | |
| | | | | | *O* | 485.9 | 1.6 | $\nu_4(MoO_4)$ |
| | | | | | *P* | 406.0 | 3.7 | |
| $E_g$ | 360 | *D* | 363.9 | 1.5 | *Q* | 368.1 | 4.2 | |
| $A_{1g}$ | 343 | *E* | 346.3 | 36.0 | | | | |
| $E_g$ | 338 | *F* | 338.3 | −5.0 | *R* | 325.4 | 2.1 | $\nu_2(MoO_4)$ |
| | | | | | *S* | 303.9 | 2.1 | |
| $E_g$ | 168 | *G* | 162.7 | 114.5 | *T* | 212.9 | 5.3 | $T'(MoO_4)*L(MoO_4)$ |
| | | | | | *U* | 189.8 | 3.1 | $T'(MoO_4)*L(MoO_4)$ |
| $A_{1g}$ | 150 | *H* | 150.2 | 26.0 | *W* | 107.4 | 4.4 | $T'(MoO_4)$ |

grid integration was used to represent the charge density. The Brillouin zone was sampled by four *k*-points generated according to the Monkhorst–Pack scheme [25]. For each value of the external hydrostatic pressure a complete conjugated gradient optimization of the atomic coordinates and the lattice parameters was performed. The optimization was interrupted when the changes both on the atomic forces and on the stress components were less than 0.05 eV/Å and $4\times10^{-4}$ eV/Å$^3$, respectively.

We have used the parameters reported for the $P\bar{3}m1$ phase of $RbFe(MoO_4)_2$ as starting structural parameters [26]. A monotonically increasing hydrostatic pressure was applied after equilibrium under atmospheric conditions. The pressure was increased up to 6.0 GPa, and after optimization we have used the Platon software developed by professor Spek [27], in order to determine the symmetry of structure in each pressure step. We observed that the optimized $RbFe(MoO_4)_2$ structure at 0.0 GPa has the $P\bar{3}m1$ space group symmetry and remains with this symmetry in the entire pressure range studied. Actually, the used computational methodology is not suitable for prediction of a phase change, and this is not the aim of this part of the present work. Therefore the fact that no phase transition was observed in our *DFT* calculations was expected, and the results obtained by us were used only for an analysis of structural properties of the trigonal phase under hydrostatic pressure.

Fig. 5 shows the calculated dependence of volume and lattice parameters with pressure. The compressibility along the *a*- and *c*-axes was determined by fitting the data to the equation:

$$r = r_0\beta P + r_0$$

with $r_0$ and $\beta$, the calculated lattice parameters at zero pressure are $a=5.743$ Å and $c=6.915$ Å whereas the respective compressibilities are $\beta_a=2.6\times10^{-3}$ and $\beta_c=7.5\times10^{-3}$ $GPa^{-1}$, respectively.

Analysis of bonds lengths and bond angles indicates that most of the bond lengths present usual behavior, i.e. they exhibit continuous decrease with the increasing pressure. Similar behavior is also observed for bond angles. However, an anomalous behavior is observed for the Mo–O1 bond, i.e. this bond length increases with the increasing pressure (see Fig. 6). It is worth noting that the observed increase in the Mo–O1 bond length is consistent with our lattice dynamics calculations and high-pressure Raman results because the 977 $cm^{-1}$ mode exhibits softening with the increasing pressure and according to our lattice

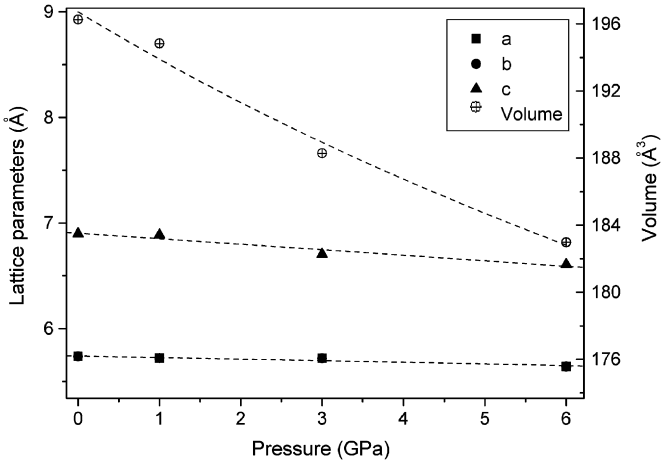


**Fig. 5.** Calculated dependence of volume and lattice parameters with pressure for $RbFe(MoO_4)_2$.

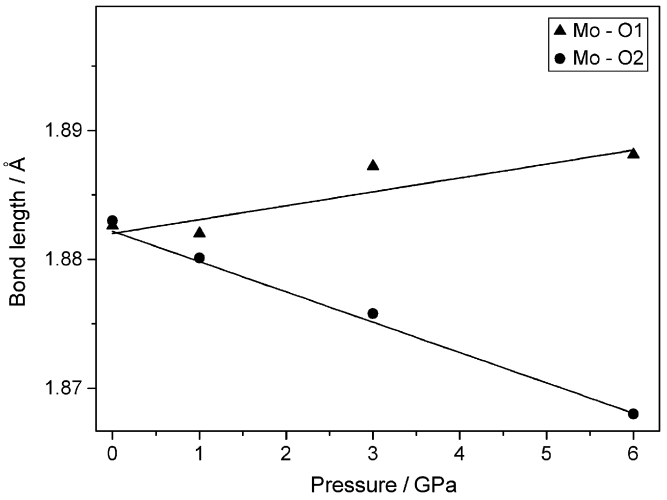


**Fig. 6.** Dependence of the Mo–O1 and Mo–O2 bonds with pressure.

dynamics calculations this mode has very large contribution of the Mo–O1 bond vibration (see Fig. 1).

### 3.4. Structural changes at the pressure induced phase transitions

Let us at first discuss the structural changes that occurred between 0 and 0.2 GPa. As mentioned above, the most characteristic change was strong intensity increase of the 360 $cm^{-1}$ band. However, no splitting of the doubly degenerate modes is observed. These results indicate that the crystal experiences weak structural changes at the phase transition and its symmetry remains trigonal. Since $RbFe(MoO_4)_2$ exhibits a temperature-induced phase transition at 190 K from the $P\bar{3}m1$ structure into another trigonal phase, it is reasonable to assume that the phase observed at 0.2 GPa and room temperature is the same as that observed below 190 K at ambient pressure. Indeed, comparison of our results with the temperature-dependent studies of $RbFe(MoO_4)_2$ shows striking similarity between our Raman spectrum recorded at 0.2 GPa and the Raman spectrum recorded below 190 K. Klimin et al. assumed that this phase transition leads to $P\bar{3}c1$ structure but our recent X-ray diffraction studies unambiguously showed that this trigonal phase has $P\bar{3}$ symmetry [12]. This result shows that the pressure dependence of $T_c$ is positive and very large, i.e. $\partial T_c/\partial p$ is higher than 500 K/GPa. It is worth noting that our previous high pressure studies of $KFe(MoO_4)_2$ also showed similar phase transition but this transition was observed at much higher pressure, i.e. at about 1.3 GPa. This results shows that the both materials exhibit similar structural instabilities under pressure. However, the stability field of the $P\bar{3}$ phase of $KFe(MoO_4)_2$ is shifted to much higher pressures and, therefore, this crystal exhibits a different sequence of temperature-induced phase transitions than $RbFe(MoO_4)_2$, i.e. instead of a transition into the $P\bar{3}$ structure, the structural instability leads to transition into ferroelastic monoclinic and triclinic phases at 312 and 139 K, respectively [1]. It is worth noting that at room temperature the $P\bar{3}$ structure is stable only in a very narrow pressure range and this pressure range is slightly larger for $RbFe(MoO_4)_2$ (about 0.4 GPa) than for $KFe(MoO_4)_2$ (less than 0.3 GPa). The comparison of the results obtained for $RbFe(MoO_4)_2$ and $KFe(MoO_4)_2$ shows also that the pressure coefficients $\alpha$ are as high as $-36.5$, 114.5 and 26.0 $cm^{-1}$/GPa for the *A*, *G* and *H* modes of $RbFe(MoO_4)_2$, respectively (see Table 4) and $-28.3$, 98.3 and 20.4 $cm^{-1}$/GPa for the corresponding modes of $KFe(MoO_4)_2$ [13]. As can be noticed these coefficients are larger for the rubidium compound since due to the larger size of the $Rb^+$ cations, when compared to the $K^+$ cations, the distance between the layers is also larger and therefore $RbFe(MoO_4)_2$ is softer than $KFe(MoO_4)_2$. The unusually high-pressure coefficients $\alpha$ indicate that pressure induces large changes in the Mo–O–Fe distances and angles due to significant rotations of $FeO_6$ octahedra and $MoO_4^{2-}$ tetrahedra.

The second transition occurs between 0.4 and 0.7 GPa and our results show that it is also very similar to that observed by us previously for $KFe(MoO_4)_2$ [13]. However, the transition pressure is much lower (between 0.4 and 0.7 GPa) than for $KFe(MoO_4)_2$ (about 1.6 GPa) [13]. Interestingly, in contrast to the $P\bar{3}$ phase the pressure coefficients $\alpha$ are smaller for the high pressure phase of $RbFe(MoO_4)_2$ when compared to the respective data found for $KFe(MoO_4)_2$. This result suggests more compact arrangement of atoms for the former compound. Regarding the structural changes that occur due to this phase transition they are certainly very large, as evidenced through drastic changes in the Raman spectra and irreversible nature of this transition. We will not discuss in detail the possible structural changes since such discussion was already presented in our previous paper for very similar high-pressure phase of $KFe(MoO_4)_2$. Here we will only mention that this phase has probably two strongly deformed, non-equivalent $MoO_4^{2-}$ units located at low symmetry sites and the structure is most likely no longer layered.

## 4. Conclusions

Lattice dynamics and *ab initio* calculations as well as pressure-dependent Raman scattering studies were performed on layered multiferroic $RbFe(MoO_4)_2$. The results show that this crystal exhibits a phase transition from the $P\bar{3}m1$ into $P\bar{3}$ structure between 0.0 and 0.2 GPa. This $P\bar{3}$ structure is the same as that observed at ambient pressure below 190 K. The second phase transition takes place between 0.4 and 0.7 GPa into a low symmetry phase. This transition is irreversible. Sequence of the pressure-induced phase transitions in $RbFe(MoO_4)_2$ is very similar to that observed for $KFe(MoO_4)_2$. However, the transitions' pressures are much lower for the rubidium compound. This result indicates that both the compounds exhibit similar structural instabilities under pressures, i.e. the phase transitions are associated with rotations of the $MoO_4^{2-}$ tetrahedra and strong deformation of the iron–oxygen and alkali-metal oxygen coordination polyhedra.

## References


[1] A.I. Otko, N.M. Nesterenko, L.V. Povstyanyi, Phys. Status Solidi A 46 (1978) 577.
[2] N.M. Nesterenko, V.I. Fomin, A.I. Zvyagin, Izv. Akad. Nauk. SSSR 43 (1979) 1675.
[3] M.B. Zapart, W. Zapart, Phase. Trans. 43 (1993) 173.
[4] G. Wang, X. Han, M. Song, Z. Lin, G. Wang, X. Long, Mater. Lett. 61 (2007) 3886.
[5] S.A. Klimin, M.N. Popova, B.N. Mavrin, P.H.M. Van Loosdrecht, L.E. Svistov, A.I. Smirnov, L.A. Prozorova, H.A. Krug van Nidda, Z. Seidov, A. Loidl, Phys. Rev. B 68 (2003) 174408.
[6] L.E. Svistov, A.I. Smirnov, L.A. Prozorova, O.A. Petrenko, L.N. Demianets, A.Ya. Shapiro, Phys. Rev. B 67 (2003) 094434.
[7] L.E. Svistov, A.I. Smirnov, L.A. Prozorova, O.A. Petrenko, A. Micheler, N. Büttgen, A.Ya. Shapiro, L.N. Demianets, Phys. Rev. B 74 (2006) 024412.
[8] T. Inami, J. Solid, State Chem. 180 (2007) 2075.
[9] A.I. Smirnov, L.E. Svistov, L.A. Prozorova, A. Zheludev, M.D. Lumsden, E. Ressouche, O.A. Petrenko, K. Nishikawa, S. Kimura, M. Hagiwara, K. Kindo, A.Ya. Shapiro, L.N. Demianets, Phys. Rev. Lett. 102 (2009) 037202.
[10] M. Kanzelmann, G. Lawes, A.B. Harris, G. Gasparovic, C. Broholm, A.P. Ramirez, G.A. Jorge, M. Jaime, S. Park, Q. Huang, A.Ya. Shapiro, A.A. Demianets, Phys. Rev. Lett. 198 (2007) 267205.
[11] M. Wierzbicka-Wieczorek, U. Kotlissch, E. Tillmanns, Z. Kristallogr. 224 (2009) 151.
[12] A. Waskowska, L. Gerward, J. Staun Olsen, W. Morgenroth, M. Maczka, K. Hermanowicz, J. Phys. Condens. Matter 22 (2010) 055406.
[13] M. Maczka, A. Pietraszko, G.D. Saraiva, A.G. Souza Filho, W. Paraguassu, V. Lemos, C.A. Perottoni, M.R. Gallas, P.T.C. Freire, P.E. Tomaszewski, F.E.A. Melo, J. Mendes Filho, J. Hanuza, J. Phys. Condens. Matter 17 (2005) 6285.
[14] J.D. Gale, J. Chem. Soc. Faraday Trans. 93 (1997) 629.
[15] E. Dowty, Phys. Chem. Miner. 14 (1987) 67.
[16] W. Paraguassu, M. Maczka, A.G. Souza, P.T.C. Freire, F.E.A. Melo, J. Mendes, Vib. Spectrosc. 44 (2007) 69.
[17] M. Maczka, W. Paraguassu, A.G. Souza Filho, P.T.C. Freire, F.E.A. Melo, J. Mendes, J. Hanuza, J. Raman Spectrosc. 36 (2005) 56.
[18] P. Hohenberg, W. Kohn, Phys. Rev. B 136 (1964) 864.
[19] P. Ordejon, J. Soler, Phys. Rev. B 53 (1996) 10441.
[20] W. Kohn, L. Sham, Phys. Rev. A 140 (1965) 1133.
[21] J. Perdew, A. Zunger, Phys. Rev. B 77 (1996) 5048.
[22] E. Artacho, D.S. Portal, P. Ordejon, A. Garcia, J. Soler, Phys. Status Solidi B 215 (1999) 809.
[23] N. Troullier, J. Martins, Phys. Rev. B 43 (1991) 1993.
[24] L. Kleinman, D.M. Bylander, Phys. Rev. Lett. 48 (1982) 1425.
[25] H. Monkhorst, J. Pack, Phys. Rev. B 13 (1976) 5188.
[26] B.G. Bazarov, R.F. Klevtsova, T.T. Bazarova, L.A. Glinskaya, K.N. Fedorov, A.D. Tsyrendorzhieva, O.D. Chimitova, Z.G. Bazarova, Rus. J. Inorg. Chem. 51 (2006) 1111.
[27] A.L. Spek, J. Appl. Cryst. 36 (2003) 7.